**Supporting Information**

# Vertical $MoS_2$ double layer memristor with electrochemical metallization as an atomic-scale synapse with switching thresholds approaching 100 mV

Renjing Xu[1,¶], Houk Jang[1,¶], Min-Hyun Lee[2], Dovran Amanov[1], Yeonchoo Cho[2], Haeryong Kim[2], Seongjun Park[2], Hyeon-jin Shin[2,*], and Donhee Ham[1,*]

[1]School of Engineering and Applied Sciences, Harvard University, Cambridge, MA 02138, USA.

[2]Samsung Advanced Institute of Technology, Samsung Electronics, Suwon 443-803, South Korea.

[¶] Renjing Xu and Houk Jang have equally contributed to this work.

* Corresponding authors: donhee@seas.harvard.edu and hyeonjin.shin@samsung.com

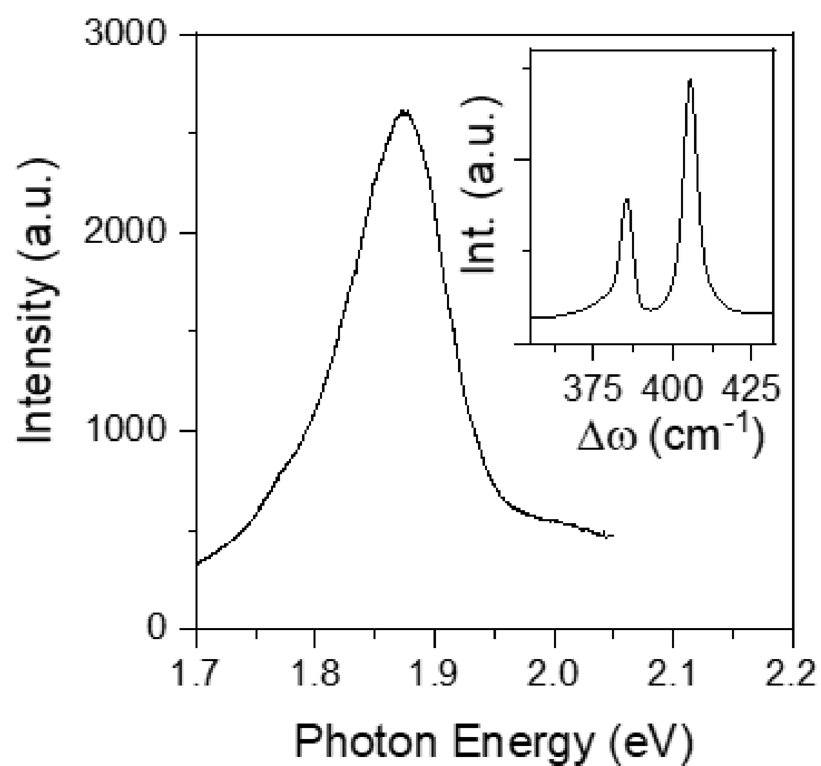


**Supplementary Figure 1.** Photoluminescence and Raman (inset) spectrum of MOCVD-grown monolayer $MoS_2$ used in our studies. It shows a photoluminescence peak at ~1.9 eV and the difference of Raman peaks of ~20 $cm^{-1}$.

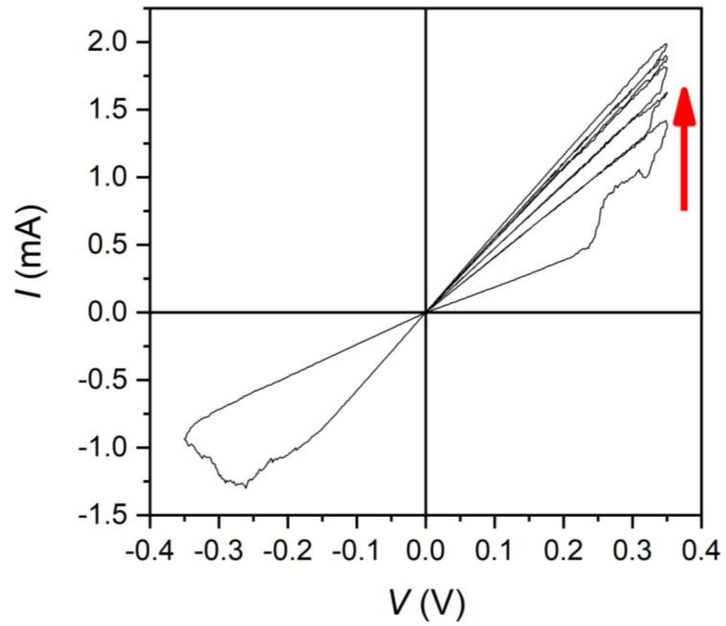


**Supplementary Figure 2.** Bipolar resistance switching. As we repeat the voltage sweep from 0 to 0.35 V, the device resistance keeps decreasing, making transitions from HRS to LRS. The device cannot be switched back to HRS with the positive voltage sweep. When the voltage is swept in the negative polarity, the device goes back to HRS.

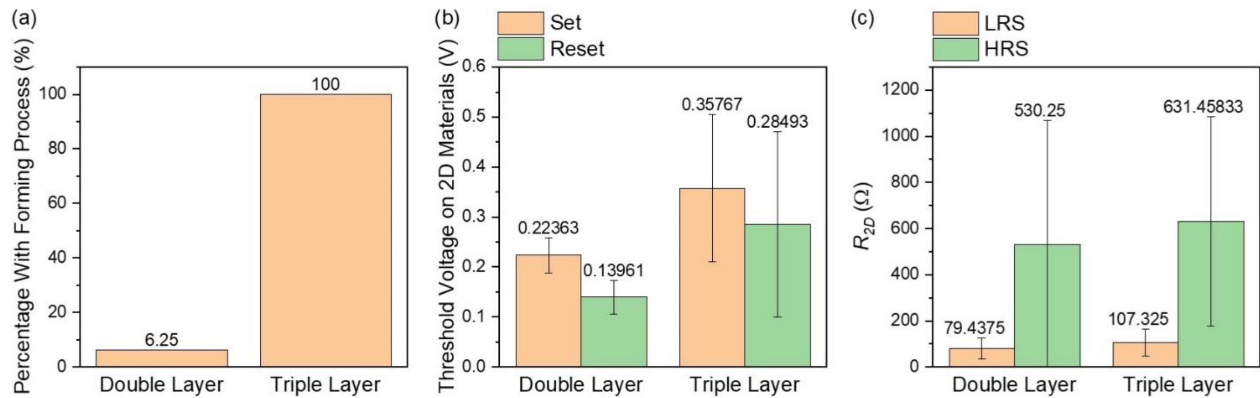


**Supplementary Figure 3.** Experimental comparison of double- vs. triple-layer $MoS_2$ memristors with bottom Au and top Cu electrodes. For the presented statistics, 16 double- and 12 triple-layer devices were measured. (a) Whereas only 1 out of the 16 double-layer devices exhibited forming process, all of the 12 triple-layer devices needed forming process. (b) The triple-layer devices tend to have higher switching voltages. (c) The difference in the HRS/LRS resistance values between the triple- and double-layer devices is not too appreciable.

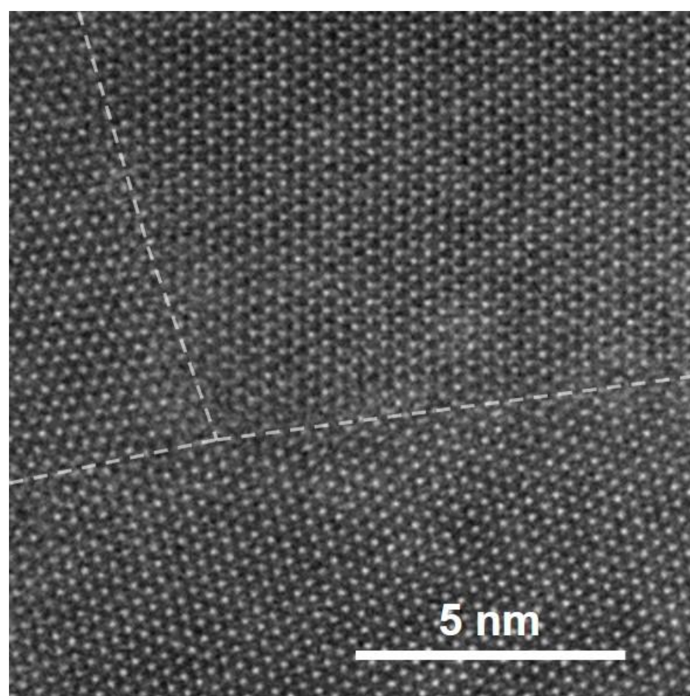


**Supplementary Figure 4.** Scanning transmission electron microscope (STEM) image—taken with high-angle annular dark-field imaging (HAADF)—of an MOCVD-grown $MoS_2$ monolayer. Grain-boundaries are evident (white-dashed lines).

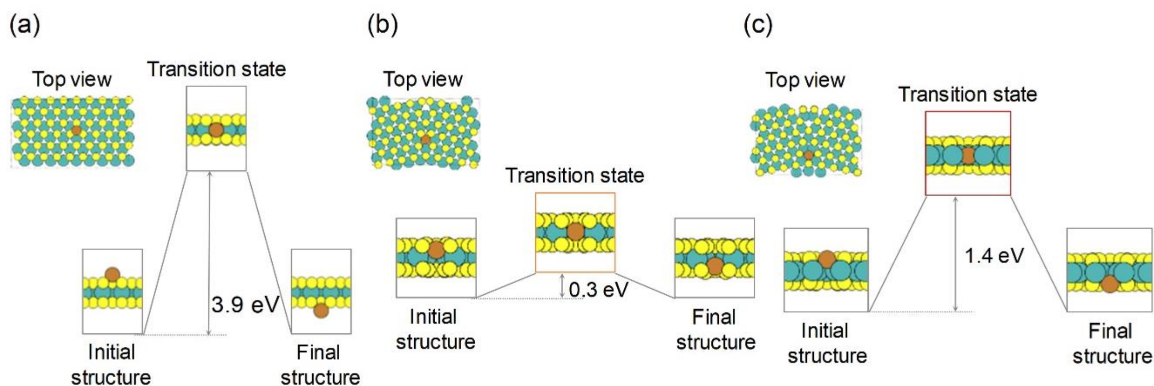


**Supplementary Figure 5.** Simulation of the energy barriers for the diffusion of Cu atoms through a crystalline $MoS_2$ monolayer and through its grain boundaries. Mo, S, and Cu atoms are shown in green, yellow, and brown, respectively. The simulation is based on the first-principle density functional theory. (a) Diffusion of a Cu atom through the crystalline $MoS_2$ should overcome a 3.9 eV energy barrier. (b) Diffusion of a Cu atom through the 3Mo+4S ring of a $MoS_2$ monolayer grain boundary involves only a 0.3 eV energy barrier. (c) Diffusion of a Cu atom through the 4Mo+3S ring of a $MoS_2$ monolayer grain boundary requires overcoming a 1.4 eV energy barrier.

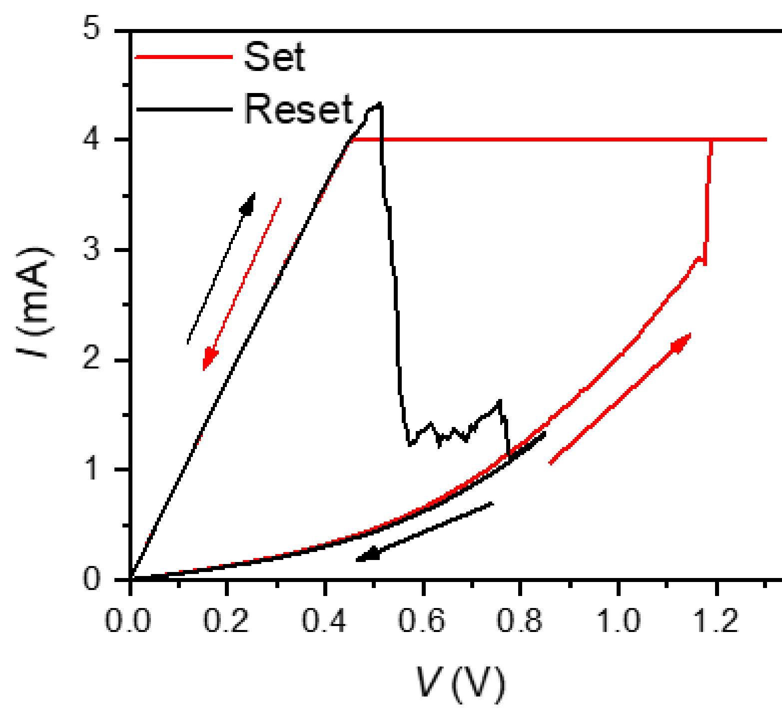


**Supplementary Figure 6.** Typical *I-V* curve for Au / $MoS_2$ double-layer / Au structure.

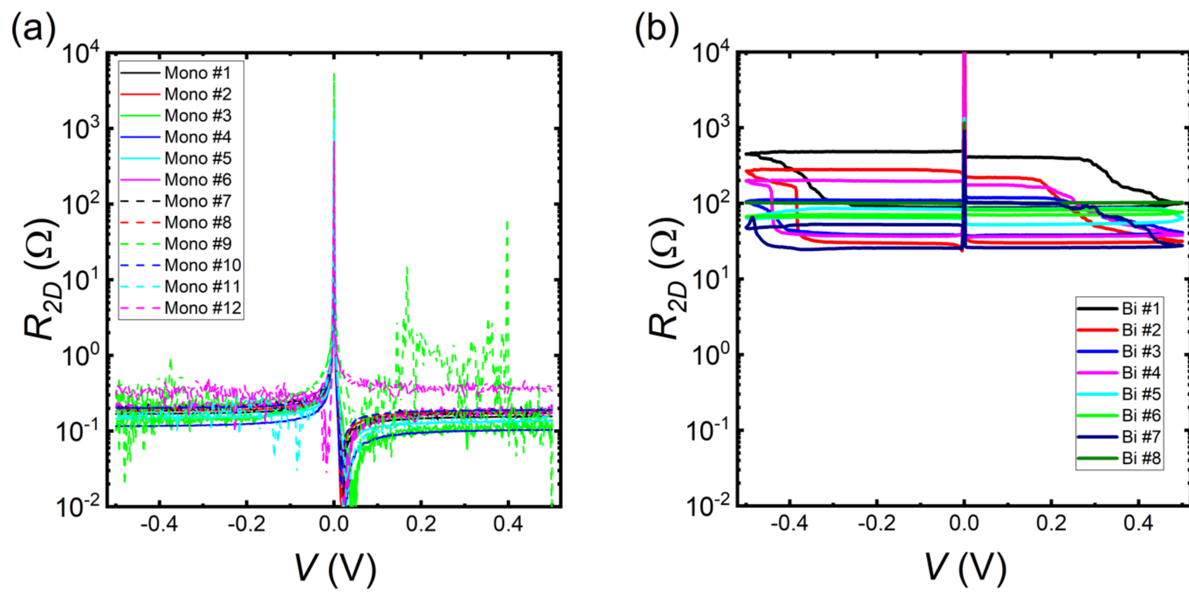


**Supplementary Figure 7.** (a) $R_{2D}$ vs $V$ obtained from four-point measurements for 12 monolayer $MoS_2$ devices and (b) 8 double-layer $MoS_2$ devices. Either type uses top Cu electrodes and bottom Au electrodes.

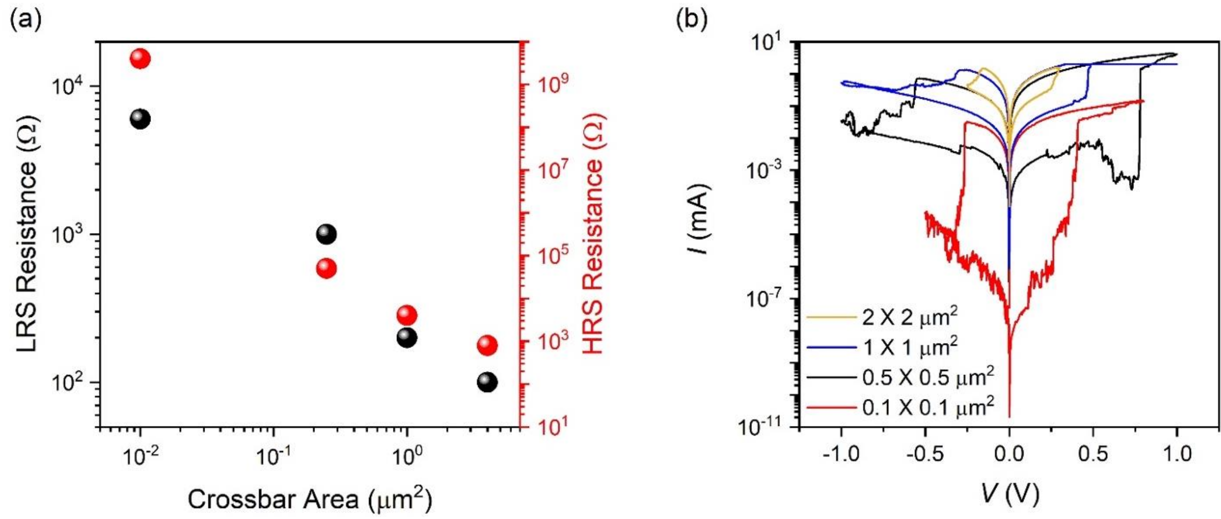


**Supplementary Figure 8.** (a) HRS and LRS resistance values and (b) typical *I-V* curves of double-layer $MoS_2$ memristors with bottom Au and top Cu electrodes with varying crossbar areas: $2 \times 2\ \mu m^2$, $1 \times 1\ \mu m^2$, $0.5 \times 0.5\ \mu m^2$, $0.1 \times 0.1\ \mu m^2$.